*American Journal of Industrial Engineering, 2013, Vol. 1, No. 3, 51-61*
Available online at http://pubs.sciepub.com/ajie/1/3/3
© Science and Education Publishing
DOI:10.12691/ajie-1-3-3

# Shliomis Model Based Ferrofluid Lubrication of Squeeze Film in Rotating Rough Curved Circular Disks with Assorted Porous Structures

**Jimit R. Patel*, Gunamani Deheri**

Department of Mathematics, Sardar Patel University, Vallabh Vidyanagar, Anand, Gujarat, India
*Corresponding author: patel.jimitphdmarch2013@gmail.com

*Received September 26, 2013; Revised December 02, 2013; Accepted December 18, 2013*

**Abstract** An endeavour has been made to analyze the effect of various porous structures on the performance of a Shliomis model based ferrofluid lubrication of a squeeze film in rotating rough porous curved circular plates. Employing the method of Christensen and Tonder's stochastic model, the roughness has been characterized by a stochastic random variable. Kozeny- Carman's model and Irmay's model for porous structures are adopted. The associated stochastically averaged Reynolds type equation has been numerically solved to obtain the pressure distribution and thus, paving the way for the calculation of load carrying capacity. The results indicate that Shliomis model based ferrofluid lubrication turns in a relatively enhanced performance as compared to Neuringer-Rosensweig model at least in the case of Kozeny- Carman's model. This investigation underlines that for the improvement in bearing performance the Kozeny- Carman's model needs to be preferred from design point of view. By suitably choosing curvature parameters and rotational inertia, the adverse effect of transverse roughness can be overcome by the positive effect of ferrofluid lubrication in the case of negatively skewed roughness when Kozeny-Carman's model is deployed.

***Keywords:*** *curved circular plates, squeeze film, roughness, magnetic fluid, Rotation, porous structures*

**Cite This Article:** Jimit R. Patel, and Gunamani Deheri, "Shliomis Model Based Ferrofluid Lubrication of Squeeze Film in Rotating Rough Curved Circular Disks with Assorted Porous Structures." *American Journal of Industrial Engineering* 1, no. 3 (2013): 51-61. doi: 10.12691/ajie-1-3-3.

## 1. Introduction

In most of the theoretical investigations of hydrodynamic lubrication it has been considered that the bearing surfaces are smooth. This appears to be an unrealistic assumption for the bearing system with lubricated film thickness. In recent years, several lubrication models accounting for surface roughness effects have been proposed in order to seek a more realistic representation of bearing surfaces. Porous structures with squeeze film characteristics play a crucial role in many applications, namely lubrication of machine elements and bearing systems. Owing to the progress of modern technology, the use of Shliomis model based magnetic fluid lubricants for squeeze film mechanisms has been highlighted.

[1] discussed the problem of squeeze film between two rotating disks, one with a porous facing. It was found that the fluid in the film region satisfied the modified Reynolds equation and the flow in the porous region satisfied Poisson's equation. [2] analyzed the effect of axial current induced pinch on the squeeze film behaviour between two annular disks and two circular disks, when the upper disc had a porous facing and the lower disc was rotated. [3] discussed the load capacity of a squeeze film between curved porous rotating circular plates. [4] theoretically analyzed the effect of squeeze film behaviour between rotating annular plates when the curved upper plates with a uniform porous facing approached normally the impermeable flat lower plate. It was concluded that the load capacity decreased when the speed of rotation of the upper disc increased up to certain value of the curvature parameter. [5] studied the effect of surface roughness on the response of a squeeze film between two rotating annular discs when one disc had a porous facing, using the stochastic theory of hydrodynamic lubrication of rough surfaces. The squeeze film behaviour between two annular discs, when the upper disc with a porous facing approached the parallel lower disc, was theoretically analysed by [6]. [7] theoretically discussed the effects of surface roughness and elastic deformation on squeeze film behaviour between rotating porous circular plates with a concentric circular pocket. [8] theoretically discussed the porous squeeze films, lubricated with a magnetic fluid in a bearing of various geometrical shapes with applied oblique magnetic fields. [9] introduced hydrodynamic lubrication of squeeze film porous bearings. It was observed that the effect of the porous layer on the hydrodynamic lubrication of squeeze film porous bearings could be neglected. [10] conducted a theoretical study of the combined effects of non-Newtonian couple stress and fluid inertia forces on the squeeze film behaviour for

parallel circular plates. The convective inertia forces included in the momentum equation were approximated by the mean value averaged across the fluid film thickness. [11] analyzed the performance of a magnetic fluid based squeeze film between porous circular plates with porous matrix of variable film thickness. It was observed that for a proper selection of thickness ratio parameter, a magnetic fluid based squeeze film bearing with variable porous matrix thickness can be made to perform considerably better than that of a conventional porous bearing with a uniform porous matrix thickness working with a conventional lubricant. [12] presented the behaviour of a magnetic fluid based squeeze film between two curved rough circular plates where in the curved upper plate lying along the surface determined by an exponential function approaches the stationary curved lower plate along the surface generated by a hyperbolic function. [13] investigated the effect of surface roughness on squeeze film behaviour between two circular disks with couple stress lubricant when the upper disk has porous facing which approaches the lower disk with uniform velocity. It was observed that the surface roughness was more pronounced as compared to classical case. [14] discussed the effect of roughness and magnetic fluid lubricant on the performance of the squeeze film formed, when the upper plate with a porous facing approached an impermeable and flat lower plate by considering the rotation of the plates. It was analyzed that the roughness required to be accounted for while designing the bearing system, even though a suitable rotation ratio parameter was chosen in the presence of a strong magnetic field. [15] modified the approach of [14] to study the performance of a magnetic fluid based squeeze film between rotating porous transversely rough circular plates with concentric circular pockets. [16] analyzed the performance of a magnetic fluid based squeeze film between rough circular plates while the upper plate had a porous facing of variable porous matrix thickness.

One of the many fascinating features of the ferrofluid is the prospect of influencing flow by a magnetic field and vice- versa. Ferrofluid is widely used in sealing of the hard disc drive, rotating x- ray tubes under engineering application and bio-medical application also. [17] presented a theoretical investigation on the effect of ferrofluid on the dynamic characteristics of curved slider bearings using Shliomis model. Shliomis model accounts for the rotation of magnetic particles, their magnetic moments and the volume concentration in the fluid. It was observed that the effect of rotation of magnetic particles improved the stiffness and damping capacity of the bearings. [18] investigated the lubrication performances of short journal bearing operating with non-Newtonian ferrofluid based upon the ferrofluid model of Shliomis and the micro-continuum theory of Stokes. It was concluded that the inclusion of non-Newtonian couple stresses signified an improvement in performance characteristics of ferrofluid journal bearings.

[19] investigated the lubrication performance of short journal bearings considering the effects of surface roughness and magnetic field. [20] analyzed the performance of a magnetic fluid based squeeze film between longitudinally rough elliptical plates. It was concluded that the increased load carrying capacity due to magnetic fluid lubricant got considerably increased due to the combined effect of standard deviation and negatively skewed roughness. All these above studies manifest that the performance of the bearing system was enhanced owing to the magnetic fluid lubricant. [21] studied the effects of velocity slip and viscosity variation in squeeze film lubrication of two circular plates. It was noticed that the load capacity and squeezing time increased due to the presence of high viscous layer near the surface and decreased owing to low viscous layer.

The aim of this paper is to extend the earlier analysis of a magnetic fluid based squeeze film between rough rotating curved circular plates studied by [22] to include the effect of Shliomis model based ferrofluid lubrication and various porous structure.

## 2. Analysis

Figure 1 shows the configuration of the curved circular disks. The bearing consists of two plates, each of radiuses $a$. The upper and lower disks rotate with angular velocities $\Omega_u$ and $\Omega_l$ respectively, about the $z$-axis. The upper disk moves normally towards the lower disk with uniform velocity $\dot{h}_0 = dh_0/dt$.

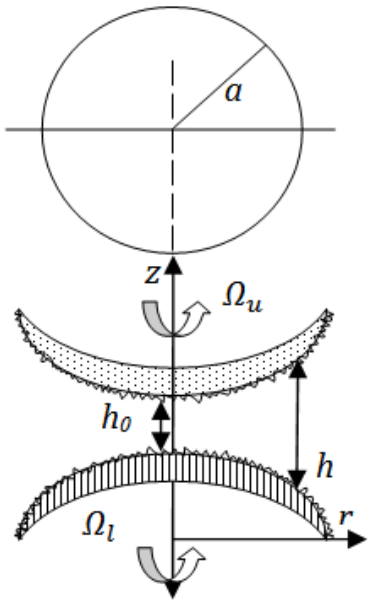


**Figure 1.** Physical Configuration of the bearing system

Employing the discussion for the stochastic modeling of transverse roughness of [23,24,25], the expression for the film thickness h(x) of the lubricant film is considered to be,

$$h(x) = \bar{h}(x) + h_s \tag{1}$$

where $\bar{h}(x)$ denote the mean film thickness and $h_s$ is the deviation from the mean film thickness characterizing the random roughness of the bearing surfaces. The deviation $h_s$ s derived by the probability density function

$$f(h_s) = \begin{cases} \dfrac{35}{32c^7}\left(c^2 - h_s^2\right)^3, & -c \le h_s \le c \\ 0, & elsewhere \end{cases}.$$

where c is the maximum deviation from the mean film thickness. The details of the mean $\alpha$, the standard deviation $\sigma$ and the parameter $\varepsilon$ which is the measure of symmetry of the random variable $h_s$, are considered from the discussion of [23,24,25].

It is assumed that the rotating upper disk lying along the surface determined by the relation

$$z_u = h_0 \exp\left(-\beta r^2\right); 0 \le r \le a$$

approaches with normal velocity $h_0'$ to the rotating lower plate lying along the surface given by

$$z_l = h_0\left[\frac{1}{1+\gamma r} - 1\right]; 0 \le r \le a$$

where $\beta$ and $\gamma$ are the curvature parameters of the corresponding plates and $h_0$ is the central film thickness. The film thickness $h(r)$ then, is defined by ([22,26])

$$h(r) = h_0\left[\exp\left(-\beta r^2\right) - \frac{1}{1+\gamma r} + 1\right]; 0 \le r \le a$$

[27] investigated that magnetic particles of a magnetic fluid can relax in two ways when the applied magnetic field changes. One is by the rotation of magnetic particles in the fluid and the other one by rotation of the magnetic moment with in the particles. Brownian relaxation time parameter $\tau_B$ gives particle rotation while the relaxation time parameter $\tau_S$ describes the intrinsic rotational process. Assuming steady flow, neglecting inertial and second derivatives of $\bar{S}$, the equations governing the flow become,

$$-\nabla_p + \eta\nabla^2\bar{q} + \mu_0\left(\bar{M}.\nabla\right)\bar{H} + \frac{1}{2\tau_S}\nabla\times\left(\bar{S} - I\bar{\Omega}\right) = 0 \quad (2)$$

$$\bar{S} = I\bar{\Omega} + \mu_0\tau_S\left(\bar{M}\times\bar{H}\right) \quad (3)$$

$$\bar{M} = M_0\frac{\bar{H}}{H} + \frac{\tau_B}{I}\left(\bar{S}\times\bar{M}\right) \quad (4)$$

Where in $\bar{S}$ is the internal angular momentum, $I$ is the sum of moments of inertia of the particles per unit volume, $\bar{\Omega} = \frac{1}{2}\nabla\times\bar{q}$, together with

$$\nabla.\bar{q} = 0, \nabla\times\bar{H} = 0, \nabla.\left(\bar{H} + \bar{M}\right) = 0$$

[26], $\bar{q}$ is the fluid viscosity in the film region, $\bar{H}$ is external magnetic field, $\bar{\mu}$ is magnetic susceptibility of the magnetic field, $p$ is the film pressure, $\eta$ is the fluid viscosity and $\mu_0$ is the permeability of the free space.

By making use of equation (3), in equation (2) and (4), one finds that,

$$-\nabla_p + \eta\nabla^2\bar{q} + \mu_0\left(\bar{M}.\nabla\right)\bar{H} + \frac{1}{2}\mu_0\nabla\times\left(\bar{M}\times\bar{H}\right) = 0 \quad (5)$$

and

$$\bar{M} = M_0\frac{\bar{H}}{H} + \tau_B\left(\bar{\Omega}\times\bar{M}\right) \quad (6)$$

Neglecting $\tau_B$ $\tau_S$ terms, substitution of $\bar{M}$ in above equation, leads to

$$\begin{aligned} &-\nabla_p + \left(\eta + \frac{\mu_0}{4}\tau_B\bar{M}.\bar{H}\right)\nabla^2\bar{q} + \mu_0\left(\bar{M}.\nabla\right)\bar{H} \\ &+\frac{1}{2}\mu_0\tau_B\begin{bmatrix}\nabla\left(\bar{\Omega}.\bar{H}\right)\times\bar{M} + \left(\bar{\Omega}.\bar{H}\right).\nabla\times\bar{M} \\ -\nabla\left(\bar{M}\bar{H}\right)\times\bar{\Omega}\end{bmatrix} = 0 \end{aligned} \quad (7)$$

From equation (6), it is easily observed that an initial approximation to $\bar{M}$ is

$$\bar{M} = M_0\frac{\bar{H}}{H}$$

Substituting the value of $\bar{M}$ on the right side of equation (6), a second approximation to $\bar{M}$ is easily seen to be

$$\bar{M} = M_0\frac{\bar{H}}{H} + \frac{M_0}{H}\tau_B\left(\bar{\Omega}\times\bar{H}\right)$$

Again, substituting this value of $\bar{M}$ on the right side of equation (6), third approximation to $\bar{M}$ is found as

$$\bar{M}.\bar{H} = M_0 H + \frac{M_0}{H}\tau_B^2\left\{\left(\bar{\Omega}.\bar{H}\right)^2 - \Omega^2 H^2\right\} \quad (8)$$

In view of the equations of Shliomis model in cylindrical polar coordinates with uniform magnetic field, when both surfaces are solid and upper one rotates, the governing equation for the film pressure is obtained from ([26]),

$$\begin{aligned} &\frac{1}{r}\frac{d}{dr}\left(\left(h^3 + 12\psi l_1\right)r\frac{dp}{dr}\right) \\ &= 12\eta_a h_0 + 24\rho\psi l_1\Omega_u^2 + \frac{3}{10}\rho\Omega_u^2\frac{1}{r}\frac{d}{dr}\left(r^2h^3\right) \\ &+\frac{3}{320}\frac{\mathrm{N}\tau_B^3}{\eta_a^3}\frac{1}{r}\frac{d}{dr}\left[h^5 r\left\{\begin{array}{l} -\left(\frac{dp}{dr}\right)^3 + \frac{27}{616}\rho^3 r^3\Omega_u^6 \\ +\frac{13}{14}\left(\frac{dp}{dr}\right)^2\rho r\Omega_u^2 \\ -\frac{251}{756}\frac{dp}{dr}\rho^2 r^2\Omega_u^4 \end{array}\right\}\right] \end{aligned} \quad (9)$$

with $l_1$ being layer thickness.

Neglecting $\tau_B^3$ term, following the discussions of [23,24,25] regarding the modelling of roughness and under the usual assumptions of hydro-magnetic lubrication ([26,28,29]) the modified Reynolds equation when both plates rotate, takes the form

$$\begin{aligned} &\frac{1}{r}\frac{d}{dr}\left(\left(g(h) + 12\psi l_1\right)r\frac{dp}{dr}\right) \\ &= 12\eta(1+\tau)h_0' + 24\rho\psi l_1\Omega_u^2 \\ &+\rho\left(\frac{3}{10}\Omega_r^2 + \Omega_r\Omega_l + \Omega_l^2\right)\frac{1}{r}\frac{d}{dr}\left(r^2 g(h)\right) \end{aligned} \quad (10)$$

where

$$g(h) = h^3 + 3h^2\alpha + 3\left(\sigma^2 + \alpha^2\right)h + 3\sigma^2\alpha + \alpha^3 + \varepsilon.$$

the following non dimensional quantities are introduced

$$\bar{h}=\frac{h}{h_0}=\left[\exp\left(-BR^2\right)-\frac{1}{1+CR}+1\right], R=\frac{r}{a},$$

$$P=-\frac{h_0^3 p}{\eta a^2 h_0}, B=\beta a^2, C=\gamma a, \bar{\sigma}=\frac{\sigma}{h_0}, \bar{\alpha}=\frac{\alpha}{h_0},$$

$$\bar{\varepsilon}=\frac{\varepsilon}{h_0^3}, \eta_a=\eta(1+\tau), \Omega_r=\Omega_u-\Omega_l, S=-\frac{\rho\Omega_u^2 h_0^3}{\eta h_0'},$$

$$\Omega_f=\frac{\Omega_l}{\Omega_u}, l^*=\frac{l}{l'}, \bar{\psi}=\frac{D_c^2 l_1}{h_0^3}, \psi^*=\frac{D_s^2 l_1}{h_0^3}, A=\frac{\bar{\psi} l^* e^3}{6(1-e)^2},$$

$$D=\frac{\psi^*\left(1-(1-e)^{\frac{2}{3}}\right)}{(1-e)}. \tag{11}$$

The relevant boundary conditions for the pressure distribution are

$$P(1)=0, \left(\frac{dP}{dR}\right)_{R=0}=0. \tag{12}$$

## 2.1. A Globular Sphere Model

In Figure 2, a porous material is filled by globular spherical particles (a mean particle size $D_c$).

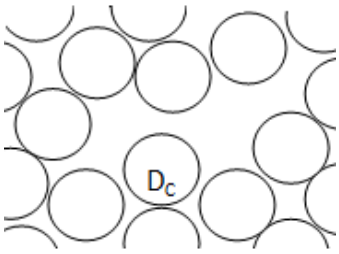


**Figure 2.** Configuration of porous structure model sheets

The Kozeny-Carman equation is well known in fluid dynamics. Relatively better results for pressure drop are obtained when this model is applied to laminar flow. [30] suggested that the use of Kozeny-Carman formula turned in the relation

$$\psi=\frac{D_c^2 e^3}{72(1-e)^2}\frac{l}{l'}$$

where $e$ is the porosity and $\frac{l}{l'}$ is the length ratio. From experimental investigations the length ratio was proposed to be around 2.5 under suitable situations. Thus, the Kozeny-Carman formula takes the form

$$\psi=\frac{D_c^2 e^3}{180(1-e)^2}$$

By making use of the boundary conditions (12) and non dimensional quantities (11), one gets the dimensionless form of the pressure distribution in the case of Kozeny-Carman, in the following form

$$P=(-6-6\tau+SA)\int_1^R \frac{R}{g(\bar{h})+A}dR + \frac{S}{10}\left(3\Omega_f^2+4\Omega_f+3\right)\int_1^R \frac{Rg(\bar{h})}{g(\bar{h})+A}dR \tag{13}$$

where

$$g(\bar{h})=\bar{h}^3+3\bar{h}^2\bar{\alpha}+3\left(\bar{\sigma}^2+\bar{\alpha}^2\right)\bar{h}+3\bar{\sigma}^2\bar{\alpha}+\bar{\alpha}^3+\bar{\varepsilon}$$

and the dimensionless load carrying capacity of the bearing system is found from

$$W=-\frac{h_0^3}{2\pi\eta a^4 h_0'}w=\int_0^1 RPdR \tag{14}$$

Therefore, the non dimensional load carrying capacity is calculated as

$$W=\left(3+3\tau-\frac{1}{2}SA\right)\int_0^1 \frac{R^3}{g(\bar{h})+A}dR - \frac{S}{20}\left(3\Omega_f^2+4\Omega_f+3\right)\int_0^1 \frac{R^3 g(\bar{h})}{g(\bar{h})+A}dR \tag{15}$$

## 2.2. A Capillary Fissures Model

The model of porous sheets, investigated by Irmay and displayed in Figure 3, consists of three sets of mutually orthogonal fissures (a mean solid size $D_s$).

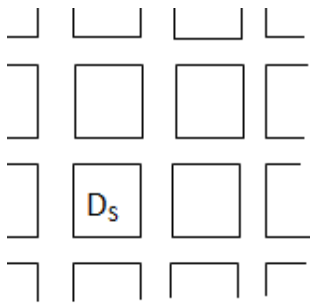


**Figure 3.** Geometry of porous Structure model sheets

Considering no loss of hydraulic gradient at the junctions, [31] presented the permeability,

$$\psi=\frac{D_s^2\left(1-(1-e)^{\frac{2}{3}}\right)}{12(1-e)}$$

where e is the porosity.

Resorting to the boundary conditions (12) and non dimensional quantities (11), the non dimensional pressure distribution for Irmay model is derived as

$$P=(-6-6\tau+SD)\int_0^R \frac{R}{g(\bar{h})+D}dR + \frac{S}{10}\left(3\Omega_f^2+4\Omega_f+3\right)\int_0^R \frac{Rg(\bar{h})}{g(\bar{h})+D}dR \tag{16}$$

In view of equation (14), the dimensionless form of load carrying capacity is calculated from

$$W = \left(3 + 3\tau - \frac{1}{2}SD\right)\int_0^1 \frac{R^3}{g\left(\bar{h}\right) + D}dR - \frac{S}{20}\left(3\Omega_f^2 + 4\Omega_f + 3\right)\int_0^1 \frac{R^3 g\left(\bar{h}\right)}{g\left(\bar{h}\right) + D}dR \quad (17)$$

## 3. Results and Discussions

It is easily noticed that equation (13) and equation (16) determine the non dimensional pressure distribution while the load carrying capacity in dimensionless form is given by equation (15) and equation (17) with respect to Kozeny- Carman's model and Irmay model respectively.

It is observed that the expressions for non dimensional load carrying capacity are linear with respect to the magnetization parameter $\tau$. Accordingly, an increase in magnetization will result in increased load carrying capacity in case of both the models. Probably, this may be due to the fact that magnetization increases the effective viscosity of the lubricant. Further a close glance at these two equations trends to suggest that the bearing can support certain amount of load even in the absence of flow unlike the case of traditional lubricants.

Setting the roughness parameters to be zero, this discussion reduces to the performance analysis of a Shliomis model based rotating porous squeeze film in smooth circular plates. In the absence of the magnetization this turns to the rotating porous squeeze film performance in curved circular plates. Further, this gives the study of [32] when there is no rotation. Lastly, taking curvature parameter to be zero, this is the effect of rotation on squeeze film performance as discussed in [1].

Figure 4 - Figure 20 and Table 1 deal with the graphical representation of Kozeny- Carman's model based porous structure while Figures 21-32 and Table 2, Table 3, Table 4 account for the case of Irmay's model based porous structure. A noticeable difference between the above two models is found from the performance points of view as can be seen from the discussions outlined below.

The Variation of the load carrying capacity presented in Figure 4 and Table 1 makes it clear that the load carrying capacity increases sharply due to the effect of magnetization.

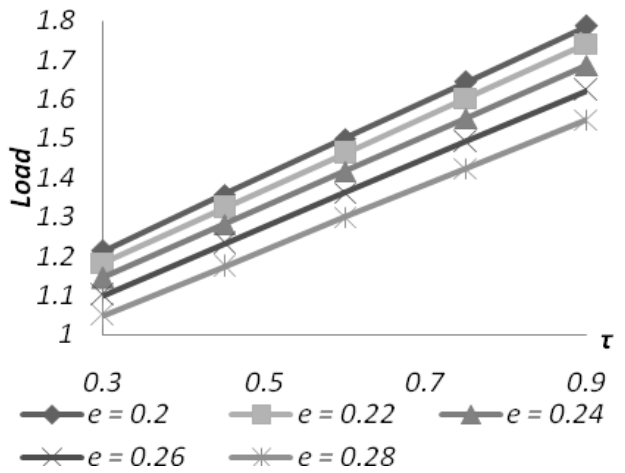


**Figure 4.** Variation of Load carrying capacity with respect to $\tau$ and e

**Table 1. Variation of Load carrying capacity with respect to $\tau$ and $\bar{\psi}$**

| $\tau$ | $\bar{\psi}$ = 25 | $\bar{\psi}$ = 30 | $\bar{\psi}$ = 35 | $\bar{\psi}$ = 40 | $\bar{\psi}$ = 45 |
|---|---|---|---|---|---|
| 0.30 | 1.18582 | 1.16533 | 1.14554 | 1.12641 | 1.10791 |
| 0.45 | 1.32567 | 1.30290 | 1.28092 | 1.25967 | 1.23912 |
| 0.60 | 1.46551 | 1.44048 | 1.41630 | 1.39293 | 1.37034 |
| 0.75 | 1.60535 | 1.57805 | 1.55168 | 1.52620 | 1.50155 |
| 0.90 | 1.74519 | 1.71562 | 1.68706 | 1.65946 | 1.63277 |

The effect of porous structures on the load distribution is presented in Figures 5-7, 20 and Tables 2-4. It is clearly seen that the porous structure effect is relatively significant in the case of Kozeny –Carman's model.

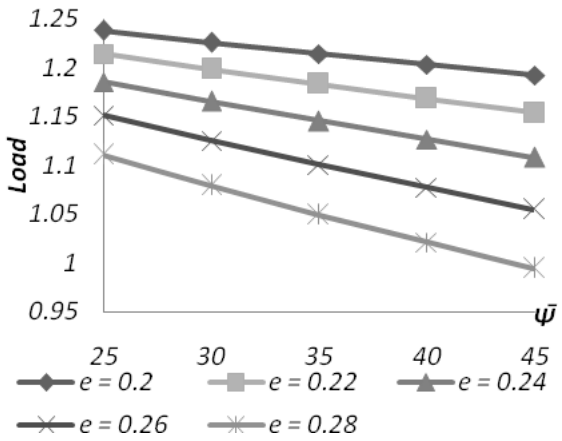


**Figure 5.** Variation of Load carrying capacity with respect to $\bar{\psi}$ and $e$

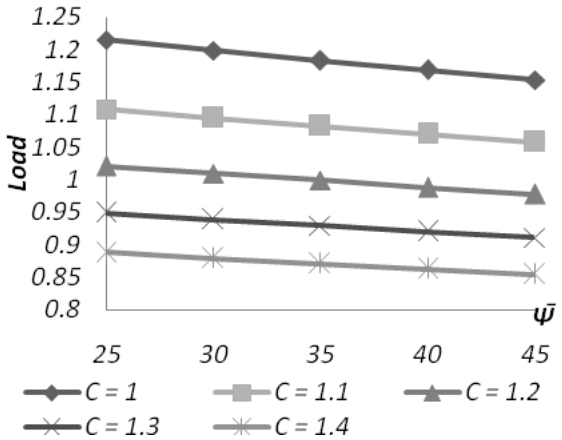


**Figure 6.** Variation of Load carrying capacity with respect to $\bar{\psi}$ and $C$

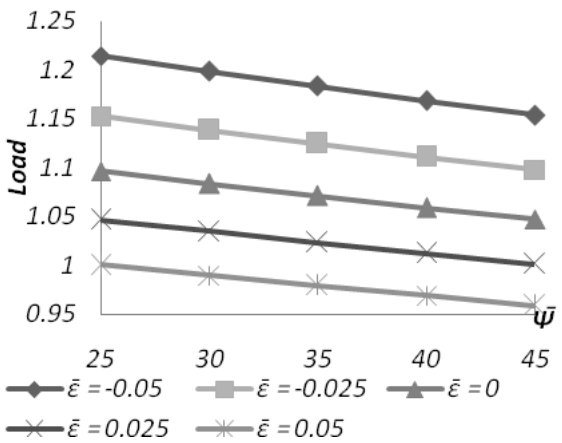


**Figure 7.** Variation of Load carrying capacity with respect to $\bar{\psi}$ and $\bar{\varepsilon}$

**Table 2. Variation of Load carrying capacity with respect to $\psi^*$ and *B***

| $\psi^*$ | B=1.5 | B=1.6 | B=1.7 | B=1.8 | B=1.9 |
|---|---|---|---|---|---|
| 1 | 0.88201 | 0.94231 | 1.00323 | 1.06450 | 1.12585 |
| 2 | 0.66345 | 0.69794 | 0.73179 | 0.76488 | 0.79712 |
| 3 | 0.52733 | 0.54962 | 0.57112 | 0.59180 | 0.61164 |
| 4 | 0.43389 | 0.44942 | 0.46423 | 0.47832 | 0.49171 |
| 5 | 0.36561 | 0.37699 | 0.38776 | 0.39794 | 0.40753 |

**Table 3. Variation of Load carrying capacity with respect to $\psi^*$ and $\bar{\sigma}$**

| $\psi^*$ | $\bar{\sigma}$ = 0.05 | $\bar{\sigma}$ = 0.1 | $\bar{\sigma}$ = 0.15 | $\bar{\sigma}$ = 0.2 | $\bar{\sigma}$ = 0.25 |
|---|---|---|---|---|---|
| 1 | 0.88201 | 0.85826 | 0.82137 | 0.77470 | 0.72186 |
| 2 | 0.66345 | 0.64960 | 0.62772 | 0.59939 | 0.56643 |
| 3 | 0.52733 | 0.51826 | 0.50380 | 0.48481 | 0.46233 |
| 4 | 0.43389 | 0.42752 | 0.41729 | 0.40373 | 0.38747 |
| 5 | 0.36561 | 0.36090 | 0.35331 | 0.34318 | 0.33093 |

**Table 4. Variation of Load carrying capacity with respect to $\psi^*$ and $\bar{\alpha}$**

| $\psi^*$ | $\bar{\alpha}$ = -0.05 | $\bar{\alpha}$ = -0.025 | $\bar{\alpha}$ = 0 | $\bar{\alpha}$ = 0.025 | $\bar{\alpha}$ = 0.05 |
|---|---|---|---|---|---|
| 1 | 0.88201 | 0.81953 | 0.76197 | 0.70897 | 0.66015 |
| 2 | 0.66345 | 0.62631 | 0.59104 | 0.55761 | 0.52599 |
| 3 | 0.52733 | 0.50273 | 0.47892 | 0.45595 | 0.43383 |
| 4 | 0.43389 | 0.41646 | 0.39936 | 0.38265 | 0.36636 |
| 5 | 0.36561 | 0.35265 | 0.33983 | 0.32718 | 0.31473 |

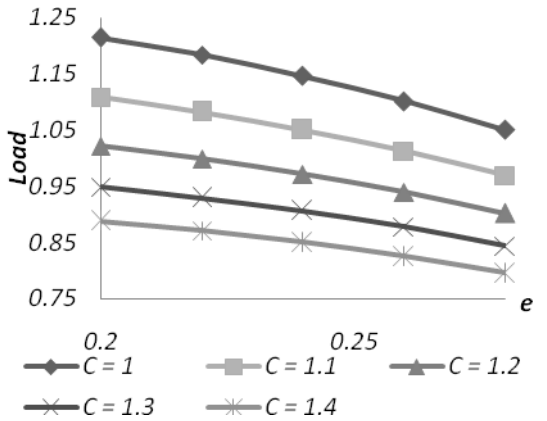


**Figure 8.** Variation of Load carrying capacity with respect to *e* and *C*

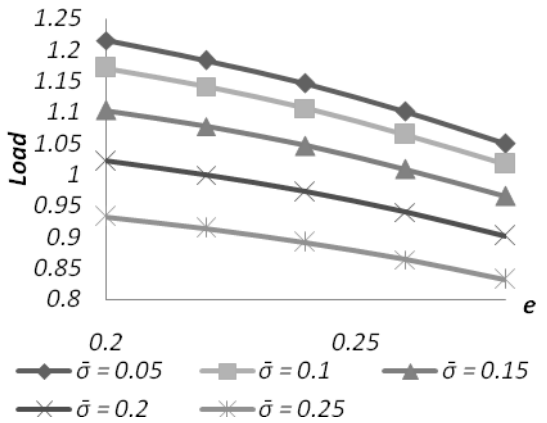


**Figure 9.** Variation of Load carrying capacity with respect to *e* and $\bar{\sigma}$

Figure 8 - Figure 11 and Figure 21, Figure 22 depict the variation of load carrying capacity with respect to the porosity parameter. It is noticed that the decrease in load carrying capacity is comparatively less in the case of Kozeny –Carman's model.

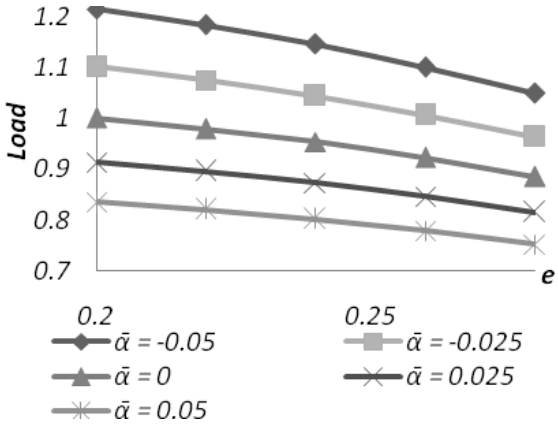


**Figure 10.** Variation of Load carrying capacity with respect to *e* and $\bar{\alpha}$

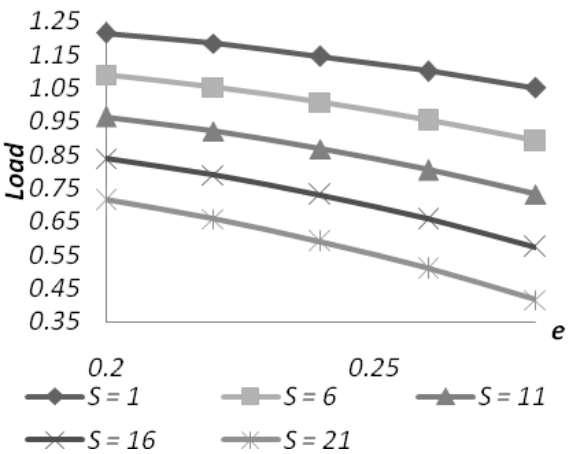


**Figure 11.** Variation of Load carrying capacity with respect to *e* and *S*

The effects of curvature parameters for both models are provided in Figure 12 - Figure 15 and Figure 23 - Figure 25. These Figures show that a proper choice of the ratio of the curvature parameters may go some way in improving the performance of the bearing system.

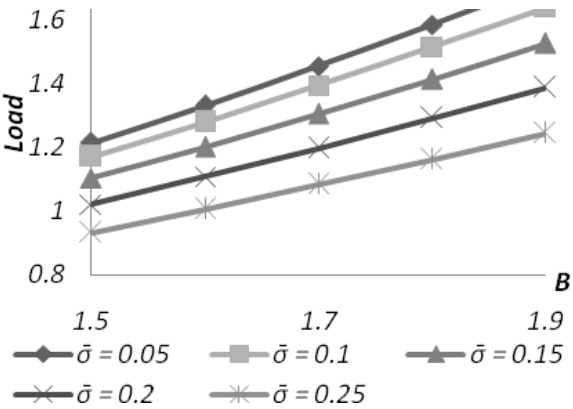


**Figure 12.** Variation of Load carrying capacity with respect to *B* and $\bar{\sigma}$

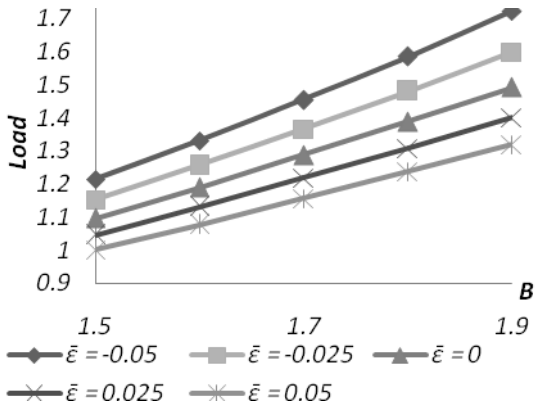


**Figure 13.** Variation of Load carrying capacity with respect to *B* and $\bar{\varepsilon}$

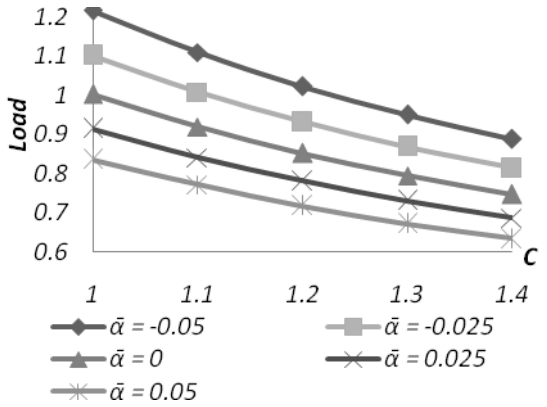


**Figure 14.** Variation of Load carrying capacity with respect to *C* and $\bar{\alpha}$

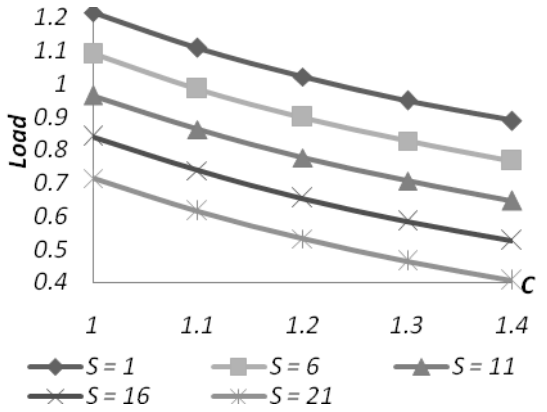


**Figure 15.** Variation of Load carrying capacity with respect to *C* and *S*

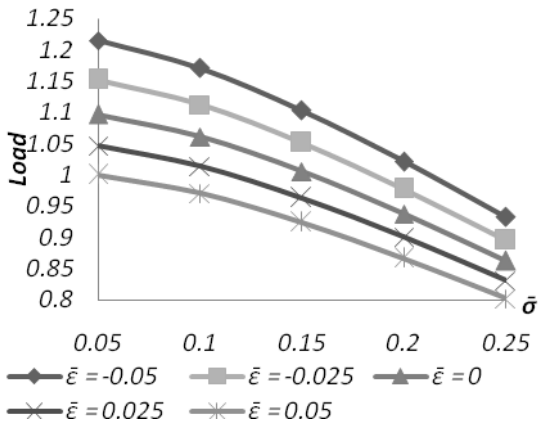


**Figure 16.** Variation of Load carrying capacity with respect to $\bar{\sigma}$ and $\bar{\varepsilon}$

The adverse effect of the standard deviation associated with roughness is shown in Figure 16 - Figure 17 and Figure 26. The rate of decrease in the load carrying capacity is more in the case of Irmay's model.

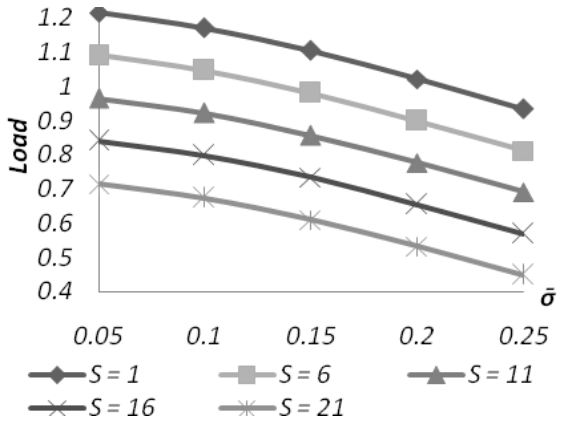


**Figure 17.** Variation of Load carrying capacity with respect to $\bar{\sigma}$ and *S*

The fact that negatively skewed roughness tends to increase the load carrying capacity is exhibited in Figure 18 and Figure 27. At the same time positively skewed roughness induces a decrease in the load carrying capacity. Furthermore, the trends of load carrying capacity with respect to variance remain identical to that of the skewness as can be seen from Figures 19 and 28.

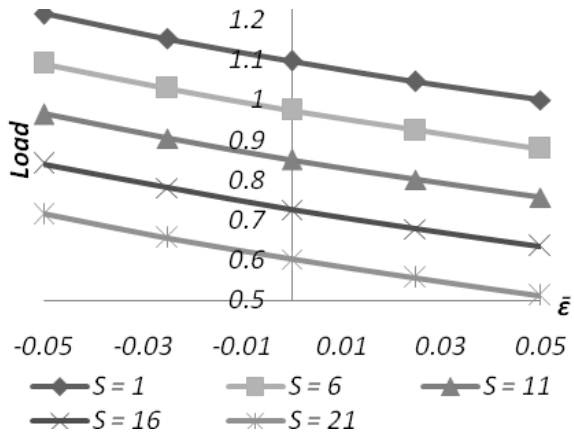


**Figure 18.** Variation of Load carrying capacity with respect to $\bar{\varepsilon}$ and *S*

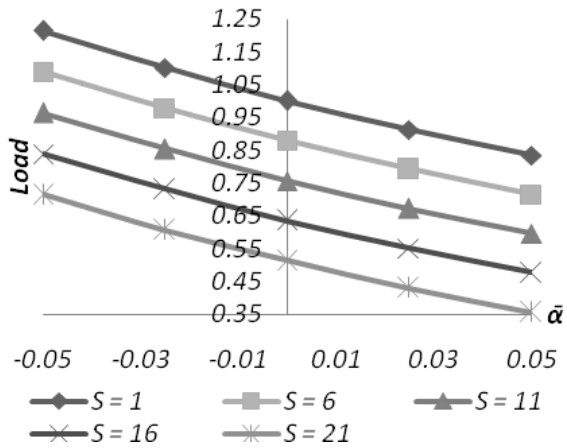


**Figure 19.** Variation of Load carrying capacity with respect to $\bar{\alpha}$ and *S*

Lastly, the effect of rotation is presented in Figure 11, Figure 15, Figure 17, Figure 18, Figure 19, Figure 20 and Figure 28. It is needless to say that for an overall improved performance, a suitable choice of rotational parameter is required.

A noticeable fact is that the compensation of the negative influence of standard deviation and porosity by the magnetization is relatively more in the case of Kozeny- Carman model when negatively skewed roughness surfaces. Of course, in this compensation the rotational inertia and curvature parameters are required to be suitably chosen.

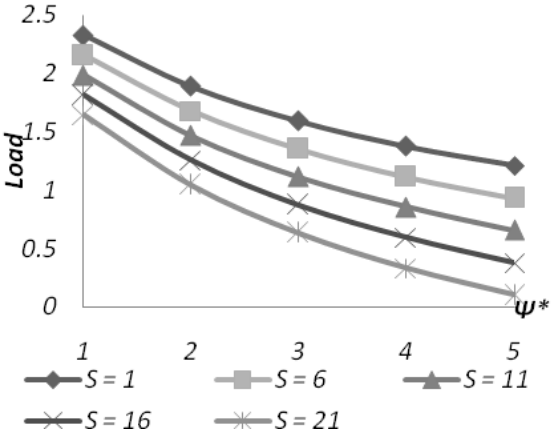


**Figure 20.** Variation of Load carrying capacity with respect to $\psi^*$ and $S$

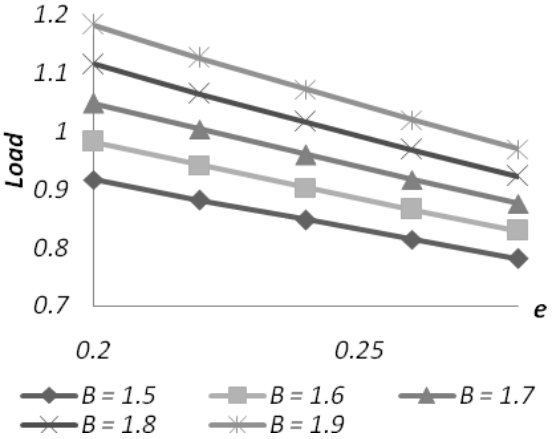


**Figure 21.** Variation of Load carrying capacity with respect to $e$ and $B$

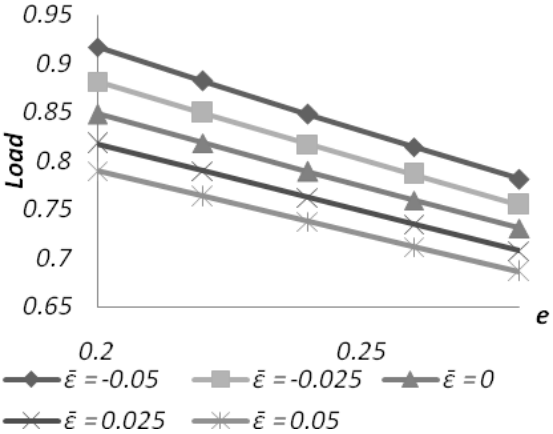


**Figure 22.** Variation of Load carrying capacity with respect to $e$ and $\bar{\varepsilon}$

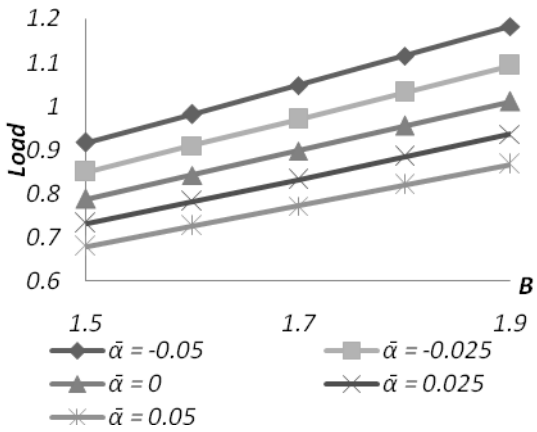


**Figure 23.** Variation of Load carrying capacity with respect to $B$ and $\bar{\alpha}$

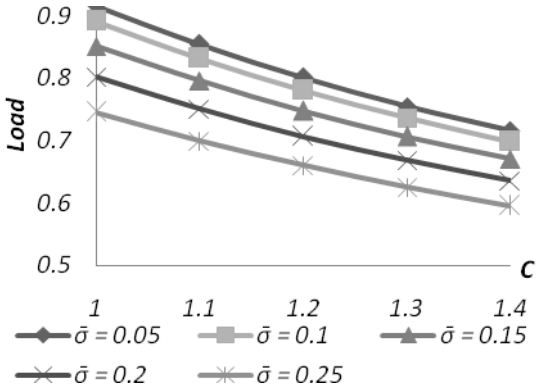


**Figure 24.** Variation of Load carrying capacity with respect to $C$ and $\bar{\sigma}$

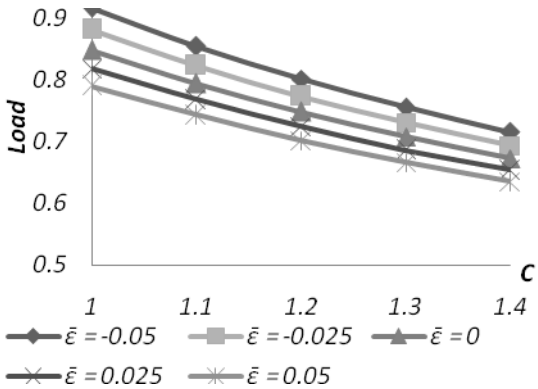


**Figure 25.** Variation of Load carrying capacity with respect to $C$ and $\bar{\varepsilon}$

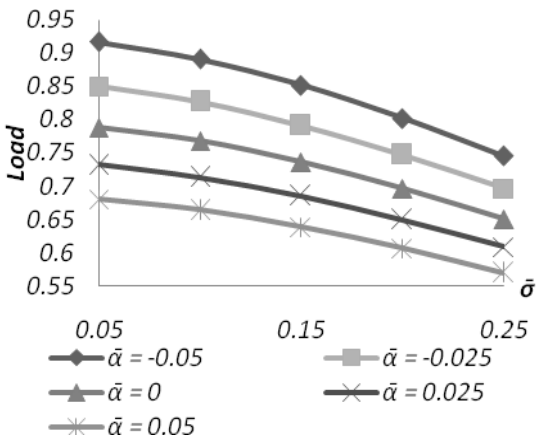


**Figure 26.** Variation of Load carrying capacity with respect to $\bar{\sigma}$ and $\bar{\alpha}$

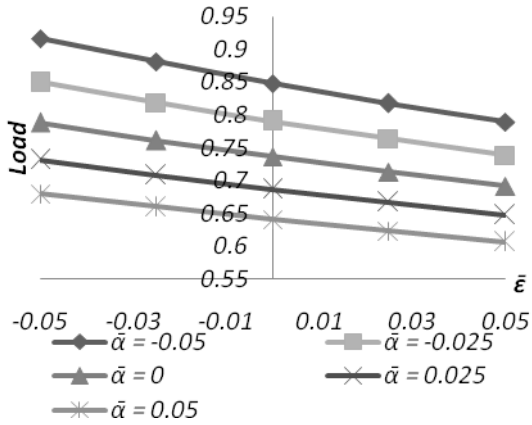


**Figure 27.** Variation of Load carrying capacity with respect to $\bar{\varepsilon}$ and $\bar{\alpha}$

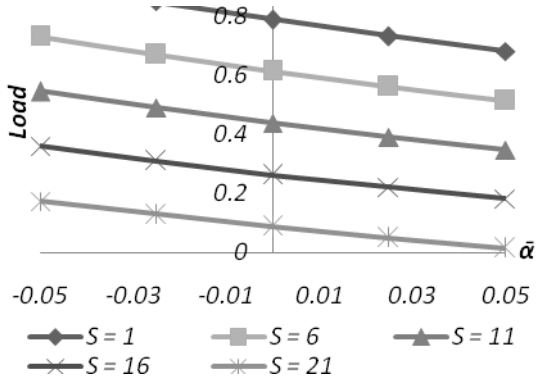


**Figure 28.** Variation of Load carrying capacity with respect to $\bar{\alpha}$ and $S$

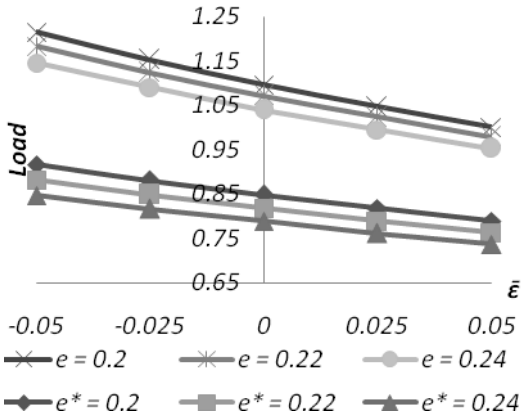


**Figure 29.** Variation of Load carrying capacity with respect to $\bar{\varepsilon}$ and porosity parameters of both the structures

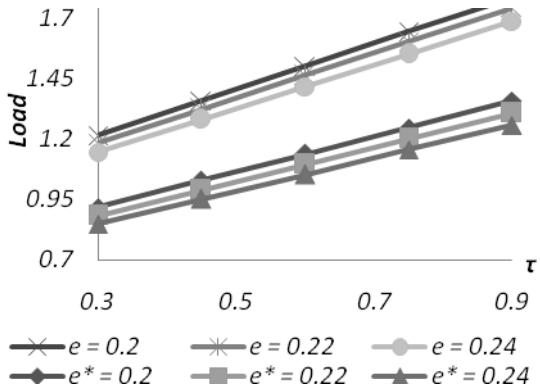


**Figure 30.** Variation of Load carrying capacity with respect to $\tau$ and porosity parameters of both the structures

A comparison between the performance analyses of both the models can be had from the Figure 29 - Figure 30 and Table 5 - Table 6. It is easily observed from these figures and tables that the Kozeny- Carman's model is a bit superior.

Here $e^*$ is the porosity parameter of Irmay's model.

**Table 5. Variation of Load carrying capacity with respect to $\bar{\varepsilon}$ and porous structure parameters of both the models**

| | $\bar{\varepsilon}$ = -.05 | $\bar{\varepsilon}$ = -.025 | $\bar{\varepsilon}$ = 0 | $\bar{\varepsilon}$ = .025 | $\bar{\varepsilon}$ = .05 |
|---|---|---|---|---|---|
| $\bar{\psi}$ = 25 | 1.2145 | 1.1524 | 1.0966 | 1.0462 | 1.0004 |
| $\bar{\psi}$ = 30 | 1.1987 | 1.1382 | 1.0838 | 1.0345 | 0.9897 |
| $\bar{\psi}$ = 35 | 1.1833 | 1.1244 | 1.0712 | 1.0231 | 0.9793 |
| $\psi^*$ = 25 | 0.0417 | 0.0414 | 0.0411 | 0.0409 | 0.0406 |
| $\psi^*$ = 30 | 0.0229 | 0.0227 | 0.0225 | 0.0224 | 0.0222 |
| $\psi^*$ = 35 | 0.0897 | 0.0088 | 0.0087 | 0.0086 | 0.0085 |

**Table 6. Variation of Load carrying capacity with respect to $\tau$ and porous structure parameters of both the models**

| | $\tau$ = 0.3 | $\tau$ = 0.45 | $\tau$ = 0.6 | $\tau$ = 0.75 | $\tau$ = 0.9 |
|---|---|---|---|---|---|
| $\bar{\psi}$ = 25 | 1.1858 | 1.3256 | 1.4655 | 1.6053 | 1.7451 |
| $\bar{\psi}$ = 30 | 1.1653 | 1.302 | 1.4404 | 1.5780 | 1.7156 |
| $\bar{\psi}$ = 35 | 1.1455 | 1.2809 | 1.4163 | 1.5516 | 1.6870 |
| $\psi^*$ = 25 | 0.0564 | 0.0716 | 0.0868 | 0.1019 | 0.1172 |
| $\psi^*$ = 30 | 0.0355 | 0.0484 | 0.0613 | 0.0742 | 0.0871 |
| $\psi^*$ = 35 | 0.0201 | 0.0313 | 0.0425 | 0.0537 | 0.0649 |

## 3.1. Validation

From the validation point of view, our results are compared with some of earlier published results. The comparison is made with the contribution of [33].

Comparison of both the models with respect to the work of [33] is provided in the following tables.

| | $\bar{\psi}$ | 25 | 30 | 35 | 40 | 45 |
|---|---|---|---|---|---|---|
| $\tau$ = 0.3 | I | 1.2378 | 1.2261 | 1.2145 | 1.2032 | 1.1921 |
| $\mu^*$ = 0.3 | II | 0.9021 | 0.8260 | 0.7627 | 0.7089 | 0.6627 |
| $\tau$ = 0.45 | I | 1.3835 | 1.3704 | 1.3576 | 1.3449 | 1.3326 |
| $\mu^*$ = 0.45 | II | 0.9024 | 0.8264 | 0.7630 | 0.7093 | 0.6631 |
| $\tau$ = 0.6 | I | 1.5291 | 1.5147 | 1.5006 | 1.4868 | 1.4732 |
| $\mu^*$ = 0.6 | II | 0.9028 | 0.8267 | 0.7634 | 0.7096 | 0.6635 |
| $\tau$ = 0.75 | I | 1.6747 | 1.6589 | 1.6436 | 1.6285 | 1.6137 |
| $\mu^*$ = 0.75 | II | 0.9031 | 0.8271 | 0.7638 | 0.7101 | 0.6638 |
| $\tau$ = 0.9 | I | 1.8203 | 1.8033 | 1.7866 | 1.7703 | 1.7543 |
| $\mu^*$ = 0.9 | II | 0.9035 | 0.8275 | 0.7642 | 0.7104 | 0.6642 |

(I - the load carrying capacity of this manuscript,
II -the load carrying capacity of [33])

| | $e$ | 0.2 | 0.22 | 0.24 | 0.26 | 0.28 |
|---|---|---|---|---|---|---|
| $\tau$ = 0.3 | I | 1.2378 | 1.2145 | 1.1858 | 1.1513 | 1.1107 |
| $\mu^*$ = 0.3 | II | 0.9021 | 07626 | 0.6389 | 0.5321 | 0.4413 |
| $\tau$ = 0.45 | I | 1.3835 | 1.3576 | 1.3257 | 1.2873 | 1.2422 |
| $\mu^*$ = 0.45 | II | 0.9024 | 0.7630 | 0.6394 | 0.5325 | 0.4416 |
| $\tau$ = 0.6 | I | 1.5290 | 1.5006 | 1.4655 | 1.4233 | 1.3738 |
| $\mu^*$ = 0.6 | II | 0.9028 | 0.7634 | 0.6397 | 0.5328 | 0.4420 |
| $\tau$ = 0.75 | I | 1.6747 | 1.644 | 1.6053 | 1.5594 | 1.5053 |
| $\mu^*$ = 0.75 | II | 0.9032 | 0.7638 | 0.6401 | 0.5332 | 0.4424 |
| $\tau$ = 0.9 | I | 1.8203 | 1.787 | 1.7452 | 1.6954 | 1.6368 |
| $\mu^*$ = 0.9 | II | 0.9036 | 0.7641 | 0.6405 | 0.5336 | 0.4428 |

Similarly the comparison with respect to the porosity parameter with regards to [33] is given in the following tables.

| | $\psi^*$ | 1 | 2 | 3 | 4 | 5 |
|---|---|---|---|---|---|---|
| $\tau$ = 0.3 | I | 0.9167 | 0.7049 | 0.5689 | 0.4738 | 0.4032 |
| $\mu^*$ = 0.3 | II | 0.2983 | 0.1698 | 0.1196 | 0.0926 | .0757 |
| $\tau$ = 0.45 | I | 1.0268 | 0.7916 | 0.6406 | 0.5349 | 0.4566 |
| $\mu^*$ = 0.45 | II | 0.2986 | 0.1702 | 0.1200 | 0.09298 | 0.0760 |
| $\tau$ = 0.6 | I | 1.1369 | 0.8783 | 0.7123 | 0.5960 | 0.5099 |
| $\mu^*$ = 0.6 | II | 0.2991 | 0.1706 | 0.1203 | 0.09335 | 0.0764 |
| $\tau$ = 0.75 | I | 1.2469 | 0.9649 | 0.7839 | 0.6512 | 0.5633 |
| $\mu^*$ = 0.75 | II | 0.2994 | 0.1710 | 0.1207 | 0.09373 | 0.0768 |
| $\tau$ = 0.9 | I | 1.3570 | 1.0515 | 0.8556 | 0.7183 | 0.6167 |
| $\mu^*$ = 0.9 | II | 0.2998 | 0.1713 | 0.1211 | 0.0941 | 0.0772 |

| | $e^*$ | 0.2 | 0.22 | 0.24 | 0.26 | 0.28 |
|---|---|---|---|---|---|---|
| $\tau$ = 0.3 | I | 0.9168 | 0.8820 | 0.8479 | 0.81426 | 0.7812 |
| $\mu^*$ = 0.3 | II | 0.2983 | 0.2706 | 0.2466 | 0.2255 | 0.2068 |
| $\tau$ = 0.45 | I | 1.0268 | 0.9882 | 0.9503 | 0.9129 | 0.8763 |
| $\mu^*$ = 0.45 | II | 0.2987 | 0.2710 | 0.2469 | 0.2258 | 0.2071 |
| $\tau$ = 0.6 | I | 1.1369 | 1.0945 | 1.0527 | 1.0117 | 0.9714 |
| $\mu^*$ = 0.6 | II | 0.2991 | 0.2713 | 0.2473 | 0.2262 | 0.2075 |
| $\tau$ = 0.75 | I | 1.2469 | 1.2007 | 1.1552 | 1.1105 | 1.0665 |
| $\mu^*$ = 0.75 | II | 0.2994 | 0.2718 | 0.2477 | 0.2266 | 0.2078 |
| $\tau$ = 0.9 | I | 1.3570 | 1.3069 | 1.2576 | 1.2091 | 1.1616 |
| $\mu^*$ = 0.9 | II | 0.2998 | 0.2721 | 0.2481 | 0.2269 | 0.2083 |

A close look at the tables reveals that the results are in good agreement.

In fact, the following points become clear.

1. It is observed that there is a limited effect of porous structure on the load carrying capacity with respect to the magnetization in the case of Kozeny- Carman's model unlike the case of Irmay's model.
2. The effect of magnetization with respect to Kozeny-Carman's model is comparatively more than the case of Irmay's model.
3. The rate of decrease in load carrying capacity due to porosity is found to be less in the case of Kozeny-Carman's model.
4. The effect of upper and lower plate's curvature parameters are found to be enhanced in the case of Kozeny- Carman's model as compared to Irmay's model.
5. The effect of standard deviation remains identical with respect to both the porous structures but the impact is sharp in Kozeny- Carman's model.
6. Positive variance and positively skewed roughness decrease the load carrying capacity while varience (-ve) and negatively skewed roughness result in increased load carrying capacity.
7. The positive effect of rotational inertia is found to be less in the case of Irmay's porous structure.

# 4. Conclusion

This study conveys that even if a suitable magnetization is in force roughness aspect must be accorded priority while designing the bearing system. Further, this investigation makes it clear that the Kozeny- Carman's model remains more suitable than the Irmay's model for designing this type of bearing system.

# Acknowledgement

The authors acknowledge with thanks the constructive comments and suggestions of both the reviewers and the editor which resulted in an overall improved presentation of the article. In fact, the comparison and validation tables are due to the suggestions of reviewers.

# References

[1] Wu, H., "The squeeze film between rotating porous annular disks", *Wear*, 18(6). 461-470. 1971.

[2] Bhat, M.V. and Patel, K.C., "The effect of axial-current-induced pinch on the lubrication of rotating porous annular and circular discs", *Wear*, 50(1). 39-46. 1978.

[3] Vora, K. H. and Bhat, M. V., "The Load capacity of a squeeze film between curved porous rotating circular plates", *Wear*, 65. 39-46. 1980.

[4] Gupta, J.L., Vora, K.H. and Bhat, M.V., "The effect of rotational inertia on the squeeze film load between porous annular curved plates", *Wear*, 79(2). 235-240. 1982.

[5] Prakash, J. and Tiwari, K., "Effect of surface roughness on the squeeze film between rotating porous annular discs with arbitrary porous wall thickness", *International Journal of Mechanical Sciences*, 27(3). 135-144. 1985.

[6] Bhat, M.V. and Deberi, G.M., "Squeeze film behaviour in porous annular discs lubricated with magnetic fluid," *Wear*, 151(1). 123-128. 1991.

[7] Prajapati, B.L., "Squeeze film behaviour between rotating porous circular plates with a concentric circular pocket: Surface roughness and elastic deformation effects", *Wear*, 152(2). 301-307. 1992.

[8] Prajapati, B.L., "Magnetic fluid based porous squeeze films", *Journal of Magnetism and Magnetic Materials*, 149. 97-100. 1995.

[9] Elsharkawy, A. A. and Nassar, M. M., "Hydrodynamic lubrication of squeeze-film porous bearings," *Acta Mechanica*, 118. 121-134. 1996.

[10] Lin, J.R., Lu, R.F., Liao, W.H. and Kuo, C.C., "Effects of couple stresses and convective inertia forces in parallel circular squeeze-film plates", *Industrial Lubrication and Tribology*, 56(6). 318-323. 2004.

[11] Deheri, G. M., Patel, H. C. and Patel, R. M., "Behaviour of magnetic fluid based squeeze film between porous circular plates with porous matrix of variable thickness", *International Journal of Fluid mechanics*, 34(6). 506-514. 2007.

[12] Deheri, G. M. and Abhangi, N. D., "Squeeze film based on magnetic fluid in curved rough circular plates", *Journal of Engineering annals of Faculty of engineering Hunedoara*, VI(2). 95-106.2008.

[13] Bujurke, N. M., Basti, D. P. and Kudenatti, R. B., "Surface roughness effects on squeeze film behaviour in porous circular disks with couple stress fluid," *Transp Porous Med*, 71.185-197. 2008.

[14] Patel, H. C., Deheri, G. M. and Patel, R. M., "Magnetic fluid-based squeeze film between porous rotating rough circular plates", *Industrial Lubrication and Tribology*, 61(3).140-145. 2009.

[15] Shimpi, M. E. and Deheri, G. M. " Surface roughness and elastic deformation effects on the behaviour of the magnetic fluid based squeeze film between rotating porous circular plates with concentric circular pockets", *Tribology in Industry*, 32(2).21-30. 2010.

[16] Patel, R. M., Deheri, G. M. and Patel, H. C., "Effect of surface roughness on the behavior of a magnetic fluid based squeeze film between circular plates with porous matrix of variable thickness", *Acta Polytechnica Hungarica*, 8(5). 171-190. 2011.

[17] Singh, Udaya P. and Gupta, R. S., "Dynamic performance characteristics of a curved slider bearing operating with ferrofluid", *Advances in Tribology*, 2012. Article Id 278723. 2012.

[18] Lin, J. R., Li, P. L. and Hung, T. C., "Lubrication performance of short journal bearing operating with non-Newtonian ferrofluids", *Z. Naturforsch*, 68a. 249-254. 2013.

[19] Hsu, T. C., Chen, J. H, Chiang, H. L. and Chou, T.L., "Lubrication performance of short journal bearings considering the effects of surface roughness and magnetic field", *Tribology International*, 61.169-175. May 2013.

[20] Andharia, P. I. and Deheri, G. M., "Performance of magnetic fluid based squeeze film between longitudinally rough elliptical plates", *ISRN Tribology*, 2013. Article Id 482604. 2013.

[21] Rao, R.R., Gouthami, K. and Kumar, J. V., "Effect of velocity-slip and viscosity variation in squeeze film lubrication of two circular plates", *Tribology in industry*, 35(1). 51-60. 2013.

[22] Abhangi, N. D. and Deheri, G. M. "Numerical modeling of squeeze film performance between rotating transversely rough curved circular plates under the presence of a magnetic fluid lubricant," *ISRN Mechanical Engineering*, 2012. Article ID 873481. 2012.

[23] Christensen, H. and Tonder, K. C., "Tribology of rough surfaces: stochastic models of hydrodynamic lubrication," *SINTEF, Report No.10*. 69-18. 1969a.

[24] Christensen, H. and Tonder, K. C., "Tribology of rough surfaces: parametric study and comparison of lubrication models," *SINTEF, Report No.22*, 69-18, 1969b.

[25] Christensen, H. and Tonder, K. C., "The hydrodynamic lubrication of rough bearing surfaces of finite width," *ASME-ASLE Lubrication Conference*, Cincinnati. OH. Paper no. 70-lub-7. October 12-15, 1970.

[26] Bhat, M. V. *Lubrication with a Magnetic fluid*, Team Spirit (India) Pvt. Ltd, 2003.

[27] Shliomis, M. I., "Effective viscosity of magnetic suspensions," *Sov. Physics JETP*, 34. 1291-1294. 1972.

[28] Prajapati, B. L. "On Certain Theoretical Studies in Hydrodynamic and Electro-magneto hydrodynamic Lubrication," *Ph. D. Thesis: S.P. University*, Vallabh Vidya- Nagar, 1995.

[29] Deheri, G. M., Andharia, P. I. and Patel, R. M., "Transversely rough slider bearings with squeeze film formed by a magnetic fluid," *Int. J. of Applied Mechanics and Engineering*, 10(1).53-76. 2005.

[30] Liu, J., "Analysis of a porous elastic sheet damper with a magnetic fluid," *Journal of Tribology*, 131.0218011-15. 2009.

[31] Irmay, S., "Flow of liquid through cracked media," *Bull. Res. Counc. Isr*, 5A (1).84. 1955.

[32] Deheri, G. M. and Patel, R. M., "The Behaviour of the squeeze film between annular plates," *Journal of engineering and technology*, 16.50-53.2003.

[33] Shah, R. C. and Patel, D. B., "squeeze film based on ferrofluid in curved porous circular plates with various porous structure," *Applied Mathematics*, 2(4). 121-123, 2012.